Theoretical study of complex resonances near ionization thresholds: Application to the N_2 photoionization spectrum

A. Giusti-Suzor and H. Lefebvre-Brion
Laboratoire de Photophysique Moléculaire du Centre National de la Recherche Scientifique, Bâtiment 213, Université Paris-Sud, 91405 Orsay Cedex, France*
(Received 22 March 1984)

A "complex" resonance, due to the autoionization of a Rydberg series close to its ionization limit perturbed by an interloper, appears frequently in photoionization spectra. This resonance structure is studied by means of an analytical formula derived from a multichannel quantum-defect treatment involving one open and two closed channels. Model calculations demonstrate the effect of the interaction between the two closed channels. Examples taken from the Ba and H_2 spectra are discussed. Finally, we reproduce the general feature of a complex resonance observed in the 785-Å region of the N_2 photoionization spectrum, using *ab initio* electronic parameters and taking account of the rotational structure.

I. INTRODUCTION

Resonant features in molecular photoionization seldomly appear as isolated resonances which could be fitted to usual Beutler-Fano profiles.[1] Owing to the multiplicity of ionization thresholds and of types of interactions (electronic, vibrational, rotational, spin-orbit) in molecules, several Rydberg series autoionize frequently in the same spectral range and the resulting resonance structure may be very intricate. Here we illustrate this point by analyzing a typical resonance figure called a "complex resonance,"[2] first noticed in H_2,[3,4,2] but common in other molecules also, for example in N_2.[5–7] It consists of an intense central peak surrounded by a broad distribution of satellites with decreasing intensity, and has been interpreted as due to the simultaneous autoionization of a dense series of Rydberg levels converging to a low-lying threshold and of a single low-n level (the "interloper") pertaining to a series with a much higher threshold. Our main purpose is to determine how both the coupling to the electronic continuum and the oscillator strength are distributed among the two series and what governs the general aspect of the complex resonance, namely, its apparent width (i.e., the total spectral range covered) as well as the individual width and intensity of each component. This study might be helpful for the identification of the interloper and of the host series in cases not yet analyzed.

We use the collisional approach of multichannel quantum-defect theory (MQDT) and restrict our model to three channels, one open, which represents the ionization continuum, and two closed, corresponding to the two Rydberg series involved. Using a variant of Seaton's MQDT[8] recently developed by Giusti-Suzor and Fano[9] and by Cooke and Cromer,[10] we derive an analytical expression for the photoionization cross section near a complex resonance. Although a three-channel model is generally a crude approximation to real processes in molecules, it is sufficient to discuss the main features of a complex resonance, and the use of an analytical formula allows very rapid and transparent model calculations. More realistic treatments including more channels can be easily handled by numerical MQDT calculations, as in the last example given in this paper (see Sec. IV C).

This analytical formula involves nine physically meaningful parameters. One of the main points which will emerge from the discussion is the important role played for the resonance structure by one of these parameters, namely, the coupling between the two closed channels. In this aspect our study may appear as a complement to the work of Mies[11] who studied, using the configuration-interaction theory, the resonant behavior of independent discrete levels coupled to several interacting continua. Here we include a single continuum in our treatment but we consider *interacting* closed channels, not assumed to be "prediagonalized."

II. MQDT ANALYTICAL DESCRIPTION OF A COMPLEX RESONANCE

A. A set of MQDT parameters

Following the MQDT approach of Ref. 9, we introduce a set of three adjusted channel wave functions $\tilde{\psi}_i$ with the long-range form (for $r > r_0$, the radius of the core region)

$$\tilde{\psi}_i = \varphi_i \tilde{f}_i - \sum_{j=1}^{3} \varphi_j \tilde{g}_j \tilde{R}_{ji} \ . \tag{1}$$

For each channel i, φ_i combines the wave functions of the ion core and of the angular and spin parts of the external electron, and $(\tilde{f}_i, \tilde{g}_i)$ denotes the phase-shifted Coulomb base pair

$$\begin{aligned} \tilde{f}_i &= f_i \cos(\pi\tilde{\mu}_i) - g_i \sin(\pi\tilde{\mu}_i) \ , \\ \tilde{g}_i &= g_i \cos(\pi\tilde{\mu}_i) + f_i \sin(\pi\tilde{\mu}_i) \ , \end{aligned} \tag{2}$$

where the effective quantum numbers $\tilde{\mu}_i$ are adjusted in order that the reaction matrix $\tilde{R}$, relative to this radial

basis, has no diagonal matrix elements ($\tilde{R}_{ii}=0$). The quantities $\tilde{\mu}_i$ replace, in effect, the diagonal matrix elements R_{ii} of Seaton's R matrix, related to $\underline{\tilde{R}}$ by Eq. (11) of Ref. 9(a). Physically, the parameters $\tilde{\mu}_i$ represent mainly the effect of the *intrachannel* short-range electron-core interactions, with a small (reactive) contribution of interchannel coupling [see Ref. 9(b)]. In real cases the $\tilde{\mu}_i$ may also contain the effect of coupling with additional channels not explicitly included in the calculations. The three other MQDT parameters introduced in Eq. (1), namely the distinct nonzero matrix elements $\tilde{R}_{ij}$ $(i<j)$, measure the interchannel couplings.

The total wave function of the system is expanded as

$$\psi=\sum_{i=1}^{3} Z_i \cos[\pi(\nu_i+\tilde{\mu}_i)]\tilde{\psi}_i \ , \tag{3}$$

with

$$\nu_1=-\tau \ , \tag{4a}$$

the open-channel phase, and 1 for $i=2,3$

$$\nu_i=\left[\frac{2\mathscr{R}}{E_i^+-E}\right]^{1/2} , \tag{4b}$$

where $\mathscr{R}$ is the Rydberg constant and E_i^+ is the ionization limit in channel i. The factors $\cos[\pi(\nu_i+\tilde{\mu}_i)]$, together with the condition $|Z_1|^2=1$ (unit flux in the single open channel), ensure the normalization per unit energy. Additional conditions on the channel components Z_i are obtained from the asymptotic behavior in each channel: convergence in each closed channel, with a standing wave in the open channel, requires that the Z_i verify the homogeneous system

$$\begin{aligned}
&-\sin[\pi(\tau-\tilde{\mu}_1)]Z_1+\tilde{R}_{12}\cos[\pi(\nu_2+\tilde{\mu}_2)]Z_2 \\
&\qquad +\tilde{R}_{13}\cos[\pi(\nu_3+\tilde{\mu}_3)]Z_3=0 \ , \\
&\tilde{R}_{12}\cos[\pi(\tau-\tilde{\mu}_1)]Z_1+\sin[\pi(\nu_2+\tilde{\mu}_2)]Z_2 \\
&\qquad +\tilde{R}_{23}\cos[\pi(\nu_3+\tilde{\mu}_3)]Z_3=0 \ , \\
&\tilde{R}_{13}\cos[\pi(\tau-\tilde{\mu}_1)]Z_1+\tilde{R}_{23}\cos[\pi(\nu_2+\tilde{\mu}_2)]Z_2 \\
&\qquad +\sin[\pi(\nu_3+\tilde{\mu}_3)]Z_3=0 \ .
\end{aligned} \tag{5}$$

The compatibility condition of this system,

$$\begin{vmatrix}
-\tan[\pi(\tau-\tilde{\mu}_1)] & \tilde{R}_{12} & \tilde{R}_{13} \\
\tilde{R}_{12} & \tan[\pi(\nu_2+\tilde{\mu}_2)] & \tilde{R}_{23} \\
\tilde{R}_{13} & \tilde{R}_{23} & \tan[\pi(\nu_3+\tilde{\mu}_3)]
\end{vmatrix}=0 \ , \tag{6}$$

yields an explicit expression of the open-channel phase τ as a function of the quantum numbers ν_2 and ν_3 and thus of the energy through Eqs. (4):

$$\tan[x_1]=\frac{\tilde{R}_{12}^2\tan[x_3]+\tilde{R}_{13}^2\tan[x_2]-2\tilde{R}_{12}\tilde{R}_{13}\tilde{R}_{23}}{\tan[x_2]\tan[x_3]-\tilde{R}_{23}^2} \ , \tag{7}$$

with the abbreviated notations $x_1=\pi(\tau-\tilde{\mu}_1)$ and $x_i=\pi(\nu_i+\tilde{\mu}_i)$ $(i=2,3)$.

The phase τ plays an important role for the analysis of the resonance structure since the resonance centers may be defined, according to Smith,[12] as the energies at which the phase varies most rapidly. It is instructive to compare Eq. (7), rewritten in the form

$$\tan[x_1]=\frac{\tilde{R}_{12}^2\cot[x_2]+\tilde{R}_{13}^2\cot[x_3]-2\tilde{R}_{12}\tilde{R}_{13}\tilde{R}_{23}\cot[x_2]\cot[x_3]}{1-\tilde{R}_{23}^2\cot[x_2]\cot[x_3]} \ , \tag{7'}$$

to the analogous two-channel expression (channel 1 open, channel 2 closed[9(a)])

$$\tan[x_1]=\tilde{R}_{12}^2\cot[x_2] \ , \tag{8}$$

to which Eq. (7') reduces if $\tilde{R}_{13}=\tilde{R}_{23}=0$. In that case the resonance centers correspond to the values $\nu_2=-\tilde{\mu}_2$ (mod 1) for which $\tan[x_1]$ tends to infinity. The inclusion of a second closed channel coupled to the first one $(\tilde{R}_{23}\neq 0)$ shifts the resonance centers near the roots of the denominator of (7'), for which

$$\tan[x_2]=\tilde{R}_{23}^2\cot[x_3] \ . \tag{9}$$

One may show that the true resonance centers, corresponding to the maximum values of the time delay $h(d\tau/dE)$,[13] are slightly shifted with respect to the roots of Eq. (9) by the *indirect* coupling between the closed channels via the continuum. This shift is negligible if $\tilde{R}_{23}^2 \ll \tilde{R}_{12}^2\tilde{R}_{13}^2$.

Equation (9) is just the MQDT relation satisfied by the level energies of the two mutually perturbed Rydberg series in channels 2 and 3. The energy range of a complex resonance covers many cycles in ν_2 but at most one in ν_3 $(\nu_2 \gg \nu_3)$, which leads to the graphical representation of Fig. 2(e), analogous to a Lu-Fano plot.[14] One sees that the roots of Eq. (9) are more and more shifted from the unperturbed resonance positions near the interloper and that one more root occurs in the vicinity of $\nu_3=-\tilde{\mu}_3$ (mod1) which marks the unperturbed energy of the interloper. Note finally that this resonance shift increases with the

closed-channel interaction $\tilde{R}_{23}$.

Besides the six MQDT parameters defined above, the expression of the photoionization cross section requires three additional short-range parameters $\tilde{D}_i$ which measure the dipole transition amplitudes corresponding to the alternative channel wave functions $\tilde{\psi}_i$. The nine short-range parameters thus introduced will be considered as *energy independent* over the spectral range covered by a complex resonance. We will see in the examples of Sec. IV that these parameters, as the usual MQDT parameters, may be either fitted from experimental spectra or derived from *ab initio* calculations. We point out that the present MQDT formulation, like the traditional configuration mixing theory, consists at least implicitly of two steps. Unperturbed, or "diabatic," channels i in a molecular designation are first defined as the eigenchannels of a "zero-order" Hamiltonian. For molecules, the corresponding channel wave functions belong to one of the Hund's cases [case (a) if the functions have the same Λ and S quantum numbers, case (d) if the rotational interactions are introduced in the zero-order Hamiltonian, or case (c) if this Hamiltonian contains the spin-orbit coupling]. The residual electrostatic interactions, treated in a second step, give rise to off-diagonal terms V_{ij} $(i\neq j)$ which are dimensionless quantities since the MQDT channel wave functions are energy normalized.

For a suitable choice of basis channels these terms will be small $(\pi\,|\,V_{ij}\,|\ll 1)$ and the quantities πV_{ij} are good approximations for the reaction matrix elements $\tilde{R}_{ij}$. The quantum defects and dipole matrix elements relative to the basis channels i are then very close to the parameters $\tilde{\mu}_i$ and $\tilde{D}_i$, respectively, as discussed in Ref. 9(b).

B. The photoionization cross section

From the total wave function (3) we derive an expression for the three-channel photoionization cross section:

$$\sigma = K\left|\sum_i Z_i \cos[\pi(\nu_i+\tilde{\mu}_i)]\tilde{D}_i\right|^2 , \tag{10}$$

where the factor K, proportional to the photon energy, does not vary much over the energy ranges considered. The channel amplitudes Z_i are solutions of the system (5), with the additional normalization condition $|\,Z_1\,|^2=1$. The cross section (10) becomes

$$\sigma = K\frac{\left[\tilde{D}_1-\left[\frac{\tilde{R}_{12}-\tilde{R}_{13}\tilde{R}_{23}\cot[x_3]}{d}\right]\cot[x_2]\tilde{D}_2-\left[\frac{\tilde{R}_{13}-\tilde{R}_{12}\tilde{R}_{23}\cot[x_2]}{d}\right]\cot[x_3]\tilde{D}_3\right]^2}{1+\{(\tilde{R}_{12}^2\cot[x_2]+\tilde{R}_{13}^2\cot[x_3]-2\tilde{R}_{12}\tilde{R}_{13}\tilde{R}_{23}\cot[x_2]\cot[x_3])/d\}^2} , \tag{11}$$

where $d=1-\tilde{R}_{23}^2\cot[x_2]\cot[x_3]$ has been already encountered in the expression (7′) of $\tan\pi(\tau-\tilde{\mu}_1)$.

This expression is the foundation of our analysis. It will be written later in a simpler form but the different terms in (11) are easily interpreted by comparison with the two-channel formula derived by Giusti-Suzor and Fano,[9(a)]

$$\sigma = K\frac{(\tilde{D}_1-\tilde{R}_{12}\cot[x_2]\tilde{D}_2)^2}{1+\tilde{R}_{12}^4\cot^2[x_2]} = K\tilde{D}_1^2\frac{(q+\epsilon)^2}{1+\epsilon^2} , \tag{12}$$

where the quantities $q=-\tilde{D}_2/\tilde{R}_{12}\tilde{D}_1$ and $\epsilon=\tan[\pi(\nu_2+\tilde{\mu}_2)]/\tilde{R}_{12}^2$ have been defined to fit the usual Fano formula. We recall that the periodic autoionization formula (12) describes at once an entire series of resonances, without the usual restriction to "isolated" resonances.

At the numerator of (11) the contribution of each closed channel $i=2,3$ to the ionization process consists of two terms. The first one, proportional to $\tilde{R}_{1i}$, corresponds to the direct path in which the absorption by a discrete level of channel 2 is "followed" by direct autoionization into the continuum. The second term, proportional to the product $\tilde{R}_{1j}\tilde{R}_{ji}$ $(j\neq i\neq 1)$, corresponds to an indirect path via the other closed channel (see Fig. 1). The two contributions are modulated by the denominator d which takes account of the mutual perturbation of both Rydberg series, as discussed previously. Moreover, the dipole amplitude $\tilde{D}_i$ of channel i is weighted by the factor $\cot[x_i]=\cot[\pi(\nu_i+\tilde{\mu}_i)]$ which becomes infinite for the unperturbed energy of each level in channel i $(\nu_i=n-\tilde{\mu}_i)$.

As in the two-channel formula (12), the denominator of (11) is simply $1+\tan^2[x_1]=1/\cos^2[\pi(\tau-\tilde{\mu}_1)]$. This term results from the normalization of the wave function (3) and determines the main features of the resonance structure. Cooke and Cromer[10] derived independently, in a similar MQDT approach, the expression of the component $|\,Z_2\,|^2$ describing the selective excitation of channel 2. Their expression, equivalent to Eq. (11) with $\tilde{D}_1=\tilde{D}_3=0$, is written as a two-channel Beutler-Fano formula with *energy-dependent* parameters q and Γ which vary rapidly in the vicinity of the interloper. Here we focus our study on the global aspect of a complex resonance, with the main purpose of learning how to identify the interloper (i.e., its unperturbed energy and width) from experimental data, a problem frequently encountered in molecules. For this purpose we now analyze some model calculations before discussing actual examples. In the following, the ionization threshold for channel 3 is assumed to lie much higher than for channel 2, such that ν_3 varies much more slowly than ν_2. Note however that Eq. (11) is symmetric with respect to channels 2 and 3 and could be used more generally to study the simultaneous autoionization of two interacting closely lying Rydberg series.

III. MODEL CALCULATIONS

Figure 2 shows the aspect of a typical complex resonance for different interaction strengths between the interloper and the host series. For reference we show first [Fig. 2(a)] the resonances obtained when a single closed channel (either 2 or 3) interacting with the open channel is included in the calculations. They have simple Lorentzian shapes because here, as in all the model calculations, we neglect the absorption by the continuum (i.e., the *direct* photoionization process) by choosing $\tilde{D}_1=0$, in order to clarify the effect of the perturbation on the resonance shapes. The cross section (11) can then be rewritten as

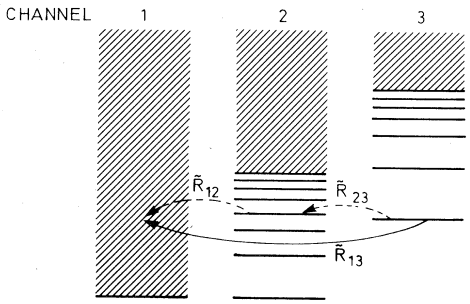

FIG. 1. Schematic representation of the three channels implied in a complex resonance. The two autoionization processes for channel 3 (→ direct path, ----→ indirect path) are indicated. An analogous scheme is valid for channel 2. The $\tilde{R}_{ij}$ are the interaction parameters between the channels.

$$\sigma=K\frac{\{\tilde{R}_{12}\tilde{D}_2\tan[x_3]+\tilde{R}_{13}\tilde{D}_3\tan[x_2]-(\tilde{R}_{13}\tilde{R}_{23}\tilde{D}_2+\tilde{R}_{12}\tilde{R}_{23}\tilde{D}_3)\}^2}{(\tan[x_2]\tan[x_3]-\tilde{R}_{23}^2)^2+(\tilde{R}_{12}^2\tan[x_3]+\tilde{R}_{13}^2\tan[x_2]-2\tilde{R}_{12}\tilde{R}_{13}\tilde{R}_{23})^2} \tag{13}$$

and is plotted in Figs. 2(b)–2(d) for different values of the effective coupling $\tilde{R}_{23}$ between the two closed channels, all the other parameters being fixed as indicated in the figure caption.

Without mutual interaction between the series [$\tilde{R}_{23}=0$, Fig. 2(b)], the interloper resonance is essentially "chopped" by the successive resonances of the host series since, as already mentioned by Fano[1] and by Mies,[11] the cross section (13) must drop to zero once between two successive autoionizing levels. The resonance structure changes radically in the more realistic case where the two closed channels are coupled, even weakly. Three main features can be noted in Figs. 2(c) and 2(d), obtained with $\tilde{R}_{23}/\pi=0.01$ and 0.02, respectively.

(i) As anticipated in Sec. II A, the autoionization peaks are very close to the roots of Eq. (9), marked by open circles in Fig. 2(e) (for $\tilde{R}_{23}/\pi=0.02$) and for which the main term in the denominator of Eq. (13) vanishes. Therefore the resonance shift increases both with the interaction strength $\tilde{R}_{23}$ between the closed channels and the proximity of the interloper.

(ii) Although there is no true background since $\tilde{D}_1=0$, the resonance shapes are no longer Lorentzian and look rather like distorted asymmetric Fano profiles with an energy-dependent background. This shape results from interferences between the direct and indirect autoionization paths mentioned in Sec. II and has been analytically studied by Cooke and Cromer.[10] The most important result of their study concerns the resonance *width* which is shown to reflect these interferences itself, resulting in a strong energy dependence clearly seen on our figures: very narrow peaks are followed by much broader ones around the interloper.

Note the narrowing of the interloper with respect to Fig. 2(a), which increases with the closed-channel coupling $\tilde{R}_{23}$. Actually, it becomes more and more difficult, to unambiguously assign one of the peaks to the interloper when the closed-channel interaction $\tilde{R}_{23}$ increases.

(iii) The most striking effect in a complex resonance is the intensity distribution which is also strongly affected by the interference effects: when the photon energy decreases, a region of very low intensity is followed by a strong enhancement of the peak maxima (the inverse situation is obtained if the relative signs of the parameters are changed). This behavior can be predicted from the cross-section values obtained when $\tan[x_2]=\tilde{R}_{23}^2\cot[x_3]$ [Eq. 9]:

$$\sigma_{\max}=K\left[\frac{\tilde{D}_2-\tilde{D}_3\tilde{R}_{23}\cot[x_3]}{\tilde{R}_{12}-\tilde{R}_{13}\tilde{R}_{23}\cot[x_3]}\right]^2, \tag{14}$$

which are very close to the true maxima of the cross section except for very small values of $\tilde{R}_{23}$ [for $\tilde{R}_{23}=0$ the constant value $\sigma_{\max}=K(\tilde{D}_2/\tilde{R}_{12})^2$, which is the peak height of the unperturbed host series, disagrees clearly with Fig. 2(b). In this case the resonance shift due to indirect coupling of the closed channels via the continuum cannot be neglected for the calculation of the maxima]. Equation (14) is represented by the dotted curves in Figs. 2(c) and 2(d). They reach the base line when

$$\tilde{D}_2=\tilde{D}_3\tilde{R}_{23}\cot[x_3], \tag{15}$$

that is, when the direct and indirect absorption processes by channel 2 interfere destructively. If by chance this point corresponds to a resonance center, the relation $\tan[x_2]=\tilde{R}_{23}^2\cot[x_3]$ transforms Eq. (15) into $\tilde{D}_3=\tilde{R}_{23}\tilde{D}_2\cot[x_2]$, which means that the absorption by channel 3 also disappears for this energy. Generally there is no resonance centered at this point but the peaks become very weak in this region. On the contrary, they are greatly enhanced around the point where

$$\tilde{R}_{12}=\tilde{R}_{13}\tilde{R}_{23}\cot[x_3] \tag{16}$$

for which $\sigma_{\max}$ becomes infinite. Here the direct and indirect couplings of channel 2 with the continuum compensate each other, resulting in a vanishing effective width and thus in a very high intensity. As above, the symmetric relation $\tilde{R}_{13}=\tilde{R}_{12}\tilde{R}_{23}\cot[x_2]$ would be satisfied simultaneously if a resonance center happens to lie at

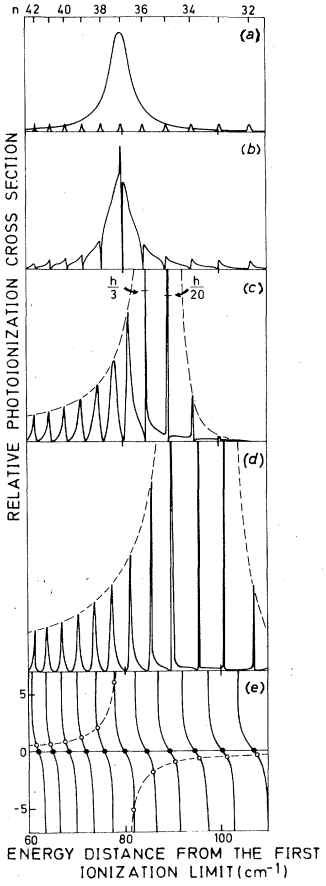

FIG. 2. (a) Two-channel calculations showing the resonance structure due to the separate interaction of each closed channel (2 or 3) with the continuum. The coupling parameters are $\tilde{R}_{12}/\pi=0.1$ (width 0.42 cm^{-1} for $n^*=32.085$) and $\tilde{R}_{13}/\pi=0.01$ (width 5.56 cm^{-1} for $n^*=2.916$). $\tilde{D}_1=0$, $\tilde{D}_2=3$ a.u., $\tilde{D}_3=10$ a.u. (b) Three-channel calculation with the same parameters as in (a). The two closed channels interact with the same continuum but are not directly coupled ($\tilde{R}_{23}=0$). (c), (d) Same parameters as in (a), with $\tilde{R}_{23}/\pi=0.01$ and 0.02, respectively. The dashed curves represent the quantity σ_{max} [Eq. (14)]. (e) For the parameters of (d), $\tan[x_2]$ (solid lines) and $\tilde{R}_{23}^2\cot[x_3]$ (dashed lines) are plotted as a function of the energy. The intersections (open circles) mark the roots of Eq. (9) and give the positions of the resonances with a very good precision. The dark circles give the unperturbed positions of the resonances in channel 2 [see (a)].

this point. Of course, infinite intensity will never occur in real cases since the corresponding infinite lifetime would be reduced by the fluorescence process, neglected in our treatment (in other words, the natural width cannot be neglected if the effective autoionization width vanishes). The possible occurrence of such a quasibound state in the continuum, stabilized by destructive interferences between two decay paths, has already been noticed by Lecomte[15] and by Cooke and Cromer.[10]

Far on the wings ($\tan[x_3]\rightarrow\infty$) the quantity σ_{max} (Eq. 14) tends to the unperturbed value $K(\tilde{D}_2/\tilde{R}_{12})^2$. The apparent width of the complex resonance, that is, the spectral range over which the host Rydberg series is perturbed,

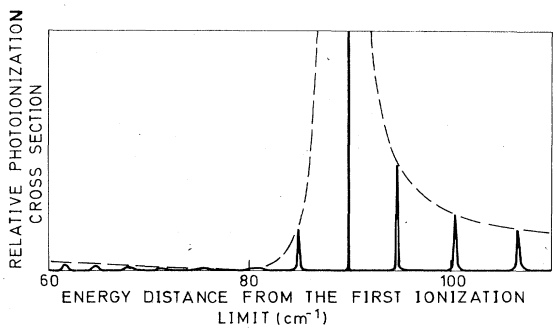

FIG. 3. Three-channel calculations with $\tilde{D}_1=0$, $\tilde{D}_2=3.0$ a.u., $\tilde{D}_3=0$, $\tilde{R}_{12}/\pi=0.1$, $\tilde{R}_{13}/\pi=0.01$, $\tilde{R}_{23}/\pi=0.01$, and the same $\tilde{\mu}$ as in Fig. 2. The scale for the photoionization cross section is also the same as in Fig. 2.

is thus approximately measured by the envelope curve σ_{max} and may be much larger than the true width of the interloper. This apparent width, as well as the shift of the higher-intensity maxima with respect to the unperturbed position of the interloper, increases with the closed-channel coupling strength $\tilde{R}_{23}$, as indicated by Eqs. (15) and (16) and by comparison between Figs. 2(c) and 2(d).

Finally, Fig. 3 corresponds to the case where $\tilde{D}_3=0$. In spite of the lack of intensity coming from the interloper, it causes a strong enhancement of the satellite peaks for long wavelengths. Beyond the interloper, the peaks are enlarged and have a vanishing intensity.

Two main results emerge from these model calculations:

(1) The spectral range covered by the complex resonance and illustrated by the curve σ_{max}, may greatly exceed the true width of the interloper.

(2) The importance of the interaction between the closed channels for the autoionization structure has been demonstrated. The interloper loses more and more of its identity when its coupling with the host series increases. Both its oscillator strength and its width are spread over the entire series. Conversely, due to the symmetry of the formula (11) in the channels 2 and 3, the interloper may borrow its intensity and/or its width from the host series, as will be seen in the example of Sec. IV C.

IV. EXPERIMENTAL EXAMPLES

The figures illustrating the previous model calculations were drawn for infinite resolution. In actual experiments, the general aspect of a complex resonance can be modified by the instrumental resolution. Particularly, the intense but very narrow peaks will be attenuated and broadened by a finite apparatus resolution. Moreover, in the case of molecular spectra where the rotational structure is not experimentally resolved, the observed peaks will consist of the superposition of numerous complex resonances, one for each value of J, the rotational quantum number. In this section we shall discuss several complex resonances observed both in atomic and molecular photoionization spectra.

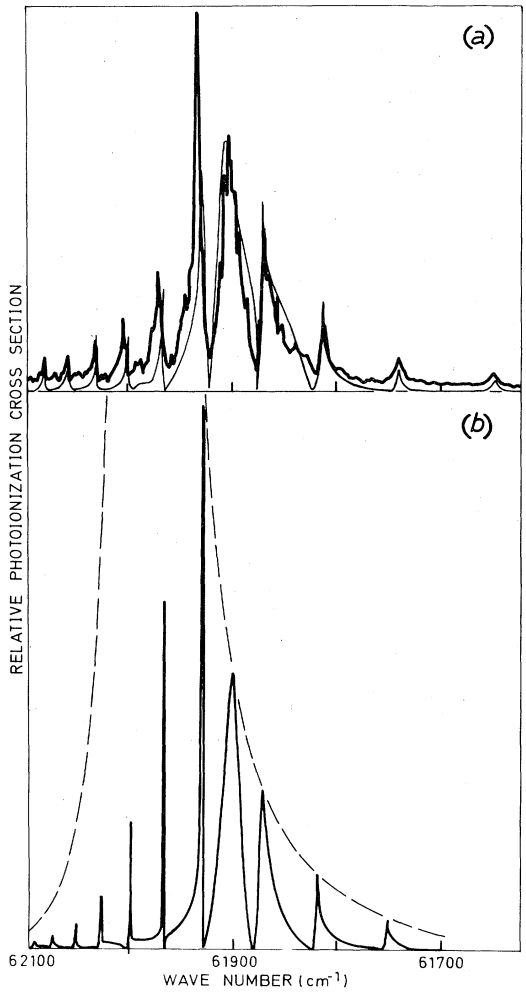

FIG. 4. (a) Experimental spectrum of the $(6p_{3/2},10d)_{J=3}$ level in Ba reproduced from Ref. 16. The continuous line shows the theoretical fit given in Sec. III G of this reference. (b) Our calculated cross section [Eq. (13)] for the same energy region with $\tilde{D}_1=\tilde{D}_2=0$, $\tilde{D}_3=10.0$ a.u., $\tilde{\mu}_2=2.79$, $\tilde{\mu}_3=2.75$, $\tilde{R}_{12}/\pi=+0.05$, $\tilde{R}_{13}/\pi=+0.1$, and $\tilde{R}_{23}/\pi=-0.08$, broadened to a resolution of 1 cm^{-1}. σ_{max} [Eq. (14)] is plotted by dashed lines.

A. The spectrum of the $(6p_{3/2},10d)_{J=3}$ level in barium

To our knowledge, the most striking example of a complex resonance in atomic photoionization spectra has been observed and extensively analyzed in Ba by Gounand *et al.*[16] In the vicinity of the $(6p_{3/2},10d)_{J=3}$ level, sharp asymmetric features appear and correspond clearly to the high members $(16\leq n\leq 26)$ of the $(6p_{1/2},nd)_{J=3}$ series, perturbed by the $(6p_{3/2},10d)_{J=3}$ interloper. The experimental spectrum is reported in Fig. 4(a) with the best theoretical fit[16] obtained in a four-channel numerical MQDT treatment based on the *eigenchannel* parameters $\{\mu_\alpha,U_{i\alpha}\}$.[17] Here we show that the main features of the experimental spectrum are reproduced by the analytical expression (13) with an alternative set of MQDT parameters, without any attempt to improve the previous fit. From arguments specific to the multistep excitation process,[18] we can assume $\tilde{D}_1\simeq\tilde{D}_2\simeq 0$. Trial values for the coupling parameters $\tilde{R}_{12}$ and $\tilde{R}_{13}$ are provided by the widths observed for the levels of each closed channel outside the range of the complex resonance. The parameters $|\tilde{R}_{23}|$, $\tilde{\mu}_2$, and $\tilde{\mu}_3$ have been deduced graphically[9(a)] from the Lu-Fano plot of the mutually perturbed series in channels 2 and 3 (Fig. 6 of Ref. 16). The minus sign for $\tilde{R}_{23}$ has been chosen in order to reproduce the very high experimental peak ($n=20$) on the correct side of the interloper.

The results, broadened to a resolution of 1 cm^{-1}, are given in Fig. 4(b). They agree reasonably well with the experimental spectrum in spite of the crudeness of the model. The strong intensities of the satellite peaks in spite of a zero oscillator strength for the $(6p_{1/2}nd)_{J=3}$ series illustrate the mechanism of intensity contamination by the interloper and of interference effects between the direct and indirect autoionization processes. Note also the narrowing of the interloper width from 55.6 cm^{-1} (its "true" width, proportional to $|\tilde{R}_{13}|^2$) to 20 cm^{-1}.

B. The $(7p\sigma\ v=2)$ level in the hydrogen molecule

In the photoionization spectrum of the H_2 molecule, reported by Dehmer and Chupka,[3] several complex resonances appear. For example, in the 791 Å spectral region, a typical complex resonance is formed by the rotational levels $J=1$ of the series $np0(v=1)$ converging to the rovibrational level $N^+=0$, $v^+=1$ of the $H_2X\,^2\Sigma_g^+$ ground state and by the interloper $(7p\sigma\ v=2)J=1$ level. This spectrum has been analyzed in detail by Jungen and Raoult[2] and their MQDT calculated spectrum, broadened to a resolution of 0.016 Å, is in good agreement with the experimental spectrum [see Fig. 5(a)]. This calculation has included 20 rovibrational channels, necessary for representing a large part of the spectrum. Here we have tried to represent schematically the small spectral range covered by this complex resonance by a three-channel calculation, with the supplementary approximations $\tilde{D}_2=0$ and $\tilde{R}_{13}=0$. Indeed, the vibrational quantum number $v=2$ of the interloper differs by two from that of the $v^+=0$ continuum such that its vibronic interaction with this continuum is very weak.[19] On the other hand, the host series in this region absorbs weakly because its levels have less favorable Franck-Condon factors than the interloper and high principal quantum numbers.

With these approximations the cross section (13) reduces to

$$\sigma=K\frac{(\tilde{D}_3\tilde{R}_{12}\tilde{R}_{23}\cot[x_3])^2}{(\tan[x_2]-\tilde{R}_{23}^2\cot[x_3])^2+\tilde{R}_{12}^4}\ . \tag{17}$$

The remaining parameters have been determined as in the preceding example: $\tilde{\mu}_2$, $\tilde{\mu}_3$, and $\tilde{R}_{23}$ are graphically read off the Lu-Fano plot drawn from the positions of the resonance peaks.[9(a)] The coupling parameter $\tilde{R}_{12}$ is deduced from the theoretical widths of the $np0(v=1)$ levels far from the interloper.[2]

The resonances in the cross section (17) are almost Lorentzian, as for an unperturbed series with no background, but the peak maxima, located on the envelope curve [dashed line in Fig. 5(b)]

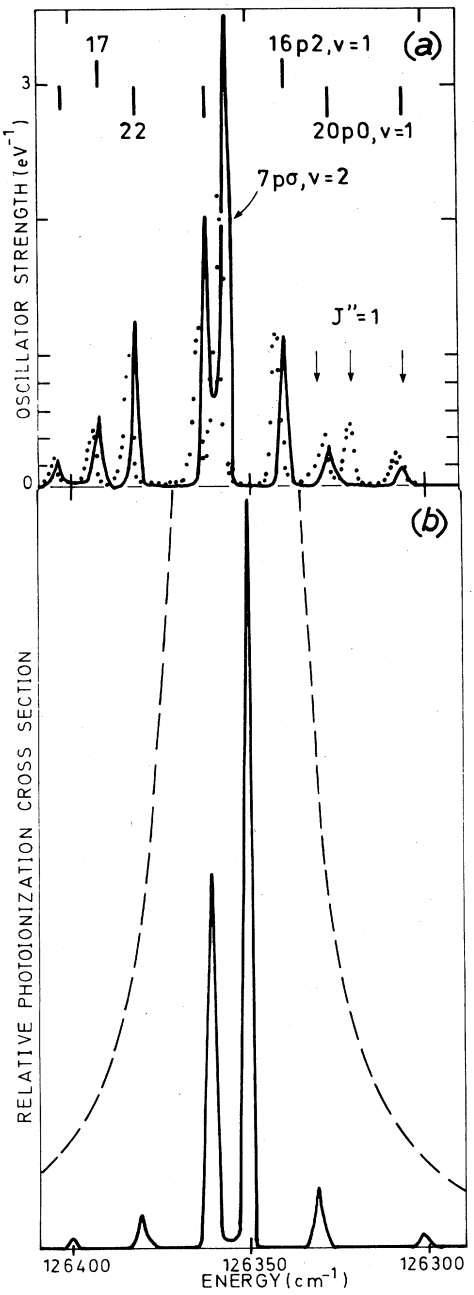

FIG. 5. (a) Observed and calculated photoionization spectra near the $v^+=1$, $N^+=0$ threshold in H_2 reproduced from Ref. 2. The experimental points are from Dehmer and Chupka (Ref. 3). (b) Our calculated cross section [Eq. (17)] for the same energy region with $\tilde{D}_1=0$, $\tilde{D}_2=0$, $\tilde{D}_3=3.16$ a.u., $\tilde{R}_{12}/\pi=0.04$, $\tilde{R}_{13}=0$, $\tilde{\mu}_2=0.08$, $\tilde{\mu}_3=0.12$, and $\tilde{R}_{23}/\pi=0.04$, broadened to a resolution of 2.6 cm^{-1}. $\sigma_{\max}$ [Eq. (14)] is plotted by dashed lines. Part of the disagreement with (a) comes from the neglect of the $np2$ channel.

$$\sigma_{\max}=K(\tilde{R}_{23}\tilde{D}_3\cot[x_3]/\tilde{R}_{12})^2 \tag{18}$$

exhibit strong variations. The same is true for the widths of the individual resonances [derived as the inverse of the maximal values of the time delay $h(d\tau/dE)$ which measures the resonance lifetime]:

$$\Gamma=\frac{4\mathscr{R}}{\pi}\frac{\tilde{R}_{12}^2}{\nu_2^3(1+\tilde{R}_{23}^4\cot^2[x_3])+\nu_3^3(1+\cot^2[x_3])\tilde{R}_{23}^2}. \tag{19}$$

Equations (18) and (19) correctly describe the distribution of intensity and width among the members of the complex resonance: in accordance with the refined MQDT calculations (see Table I of Ref. 2), the highest peaks are the closest to the unperturbed position of the interloper ($\cot[x_3]\to\infty$) and have the smallest widths.

The cross section, calculated by means of Eq. (17) and broadened to the experimental resolution of 2.6 cm^{-1}, is shown in Fig. 5(b). It is clear that with this very schematic model, we reproduce at least the two main characteristics of this spectrum, already pointed out by Jungen and Raoult:[3] the intensity of the satellite peaks comes from the interloper, which in turn borrows its width from the levels of the host series. Note that the calculated widths before convolution are all much smaller than the experimental resolution width, such that all the peaks in the experimental spectra and the two convoluted theoretical spectra have an apparent width of about 2.6 cm^{-1}.

In this example the interactions $\tilde{R}_{12}$ and $\tilde{R}_{23}$ responsible both for the autoionization of the host series and for the redistribution of the oscillator strength have the same vibronic origin and the same order of magnitude. Several other cases of complex resonances have been pointed out in H_2.[3,4] Their mechanisms may be more complicated. For example, in the 803-Å region, two kinds of interactions, electron-rotation and electron-vibration couplings, are implied and there is a transfer between these two coupling modes. Effective parameters $\tilde{\mu}_i$ and $\tilde{R}_{ij}$ can still be defined but the three-channel formula would be only valid in a very small energy range because two interlopers are actually involved. The same situation is encountered in the following example.

C. The Worley-Jenkins series near the 783.5-Å region in the nitrogen molecule spectrum

In the photoionization spectrum of N_2 observed at high resolution by Dehmer *et al.*,[6] a complex resonance appears near 783.5 Å, just below the ionization limit $v^+=1$ of the $X\,^2\Sigma_g^+N_2^+$ state. This complex resonance has been previously interpreted by us[5,20] as due to the interaction between the $5s\sigma_g\,^1\Pi_u$ member of Worley's third series converging to the $v^+=0$ $A\,^2\Pi_uN_2^+$ limit and the higher members ($m=n-1\geq 15$) of the $np\pi_u\,^1\Pi_u$ Worley-Jenkins series converging to the $v^+=1$ $X\,^2\Sigma_g^+$ level. These members present an anomalous enhancement of their intensity near the interloper. The interaction between these states has the same electrostatic origin as the interaction between the $5s\sigma g\,^1\Pi_u$ state and the continuum of the $v^+=0$ $X\,^2\Sigma_g^+$ level responsible for the autoionization of this state. Even if the direct vibrational coupling of the members of the Worley-Jenkins series with the continuum $v^+=0$ is neglected, we have shown that the indirect interactions via the $5s\sigma_g\,^1\Pi_u$ state is sufficient to reproduce qualitatively the observed intensity anomaly.

Actually, this complex resonance contains two interlopers attributed by Ogawa and Tanaka[21] to two members of

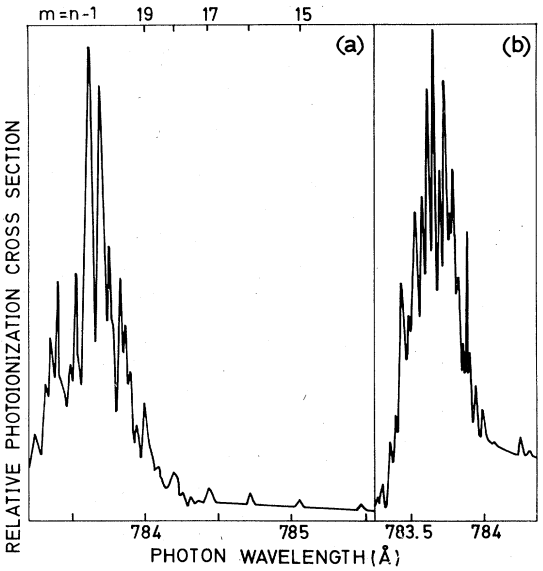

FIG. 6. (a) Experimental photoionization cross-section of N_2 taken with a wavelength resolution of 0.017 Å near the N_2^+ $X\,^2\Sigma_g^+(v^+=1)$ ionization threshold (Ref. 6). The absorption spectrum suggests that the wavelength calibration requires a shift of 0.02 Å to the red. (b) Calculated photoionization cross section with a MQDT calculation including the band contour and broadened to a resolution of 2.5 cm^{-1}. The parameters are given in Table I.

Worley's (third) Rydberg series converging to different vibrational levels of the $A\,^2\Pi_u$ state of N_2^+. A further complication arises from the rotational structure which is partially resolved and cannot be neglected. Indeed, the R- and Q-branch heads of each of the $^1\Pi_u \leftarrow X\,^1\Sigma_g^+(A\,^2\Pi_u)ns\sigma_g$ transitions, separated by 14 cm^{-1}, can be seen on the experimental figure 6(a). Furthermore, each member of the Worley-Jenkins series forms a p complex whose $^1\Sigma_u^+$ and $^1\Pi_u$ parts are completely mixed. Thus, we have studied this problem again including the two interlopers and taking into account the rotational structure in a simplified form. For the p complex, we have considered only the $\Delta N^+=0$ (Q-form) branches. The Π-Σ separation of the components of each complex has been taken equal to zero. This is justified by the experimental observation[22] of the members with $n>15$ of the series converging to $v^+=0$ of $X\,^2\Sigma_g^+$. The f complexes have been treated in the same way as the p complexes. As the temperature is 78 K, there is only adequate population up to the $J=8$ rotational level. The rotational constants have been taken as 2.0 cm^{-1} for $X\,^1\Sigma_g^+$, 1.902 cm^{-1} for $X\,^2\Sigma_g^+$, and 1.739 cm^{-1} for $A\,^2\Pi_u$. The main features of the complex resonance depend drastically on the exact values of the quantum defects of the two interlopers. The experimental relative intensity of the two parts of the resonance is only reproduced if the $(v=0,n=4)$ $5s\sigma_g$ interloper is placed at higher energy than the $(v=3,n=3)$ $4s\sigma_g$ interloper. The values of the quantum defects of these interlopers have been adjusted separately with a preliminary model including only three channels at the same time, namely, one of the interloper channels and the two p channels (with $v^+=0$ and 1), but in different energy regions of the complex resonance. It has thus been possible to use the formula (11) for each value of J and separately for each ensemble of P, R, and Q lines.

The $\tilde{D}_i$ and $\tilde{R}_{ij}$ electronic parameters have been taken from *ab initio* calculations[7] except that the interaction between the closed channels $(A\,^2\Pi_u)\epsilon s\sigma$ and $(X\,^2\Sigma_g^+)\epsilon p\pi$ has been multiplied by a factor of 2, becoming equal to the calculated interaction between the $(A\,^2\Pi_u)\epsilon s\sigma$ and $(X\,^2\Sigma_g^+)\epsilon f\pi$ closed channels. These electronic parameters (two interaction parameters and three transition moments) have been weighted by the corresponding overlaps between the vibrational levels of the Morse potential curves. The vibrational coupling between the $v^+=0$ and $v^+=1$ $X\,^2\Sigma_g^+$ channels has been neglected. The quantum defect for $(X\,^2\Sigma_g^+)\epsilon p\pi$ has been taken from experiment and that for $(X\,^2\Sigma_g^+)\epsilon f\pi$ from calculations [the experimental value 0.0233 for $4f$ (Ref. 23) differs insignificantly from the calculated value 0.0168]. All these parameters are given in Table I. They have been introduced in a model with six channels [two (p and f) open channels, four closed channels] for which the analytical formula (11) is no longer valid. We have then solved the electronic autoionization MQDT equations[5] for each ensemble of P, R, and Q transitions and this, for each value of J. The sum has been broadened to the resolution of 2.5 cm^{-1}. The final results are reproduced in Fig. 6(b). We see that without any further adjustment of the parameters, the appearance of the complex resonance is correctly represented. In particular, the anomalous enhancement of the p members of the Worley-Jenkins series far from the interlopers are well reproduced and although the vibrational interaction between the $v^+=0$ and 1 channels of the $X\,^2\Sigma_g^+$ state has been neglected (corresponding to put $\tilde{R}_{12}=0$ in the model), both the p and f levels are enlarged by indirect

TABLE I. Parameters used in the calculation of the N_2 complex resonance.

Channel	$(X\,^2\Sigma_g^+\ v^+=0)$ $\epsilon p\pi_u$	$(X\,^2\Sigma_g^+\ v^+=0)$ $\epsilon f\pi_u$	$(X\,^2\Sigma_g^+\ v^+=1)$ $\epsilon p\pi_u$	$(X\,^2\Sigma_g^+\ v^+=1)$ $\epsilon f\pi_u$	$(A\,^2\Pi_u\ v^+=0)$ $\epsilon s\sigma_g$	$(A\,^2\Pi_u\ v^+=3)$ $\epsilon s\sigma_g$
$\tilde{\mu}$	−0.36	0.0168	−0.36	0.0168	0.0664	0.0553
$\tilde{D}$ (a.u.)	−0.702	−0.316	−0.207	−0.0937	−0.197	−0.124
$\underline{R}$	0	0	0	0	−0.0137	−0.0039
		0	0	0	−0.0137	−0.0039
			0	0	0.0118	−0.0086
				0	0.0118	−0.0086
					0	0.0
						0.0

electronic coupling.

We note that the calculated electronic parameters (transition moments and interaction) are in good agreement with the known semiempirical values.[24] In particular, our calculated electronic interaction between the $(A\,^2\Pi_u)\epsilon s\sigma_g$ and $(X\,^2\Sigma_g^+)\epsilon p\pi_u$ channels of -0.0097 is of the same order of magnitude as the value 0.0062 deduced from the work of Stahel *et al.*,[24] but disagrees with the value 0.085 used in our previous work[20] where we have confused the apparent width of the complex resonance with the true width of the interloper.

Furthermore, we have looked for an explanation of the low intensity observed for the members $m=9-11$ of this same Worley-Jenkins series and pointed out by Dehmer *et al.*[6] The zero value for the cross section resulting from interference effects [see Eq. (15)] cannot occur so far from this interloper with the small values of our closed-channel interaction parameters. But other features seen at 791 and 792 Å, which we suggest to correspond to the enhancement of the $9f$ complex by the $(A\,^2\Pi_u)3d\delta_g$ $v=2$ interloper and of the $8p$ complex by the $(A\,^2\Pi_u)3d\sigma_g$ $v=1$ state, respectively, could be responsible in part for the intensity anomaly of these $m=9-11$ members. The strong calculated electronic interactions between the closed channels[7] seem to support this explanation.

In this part of the spectrum of N_2, a single continuum is open. Higher in energy, the situation becomes more and more complicated, due to numerous close ionization thresholds. For example, the first member of the Hopfield absorption series corresponding to the $(B\,^2\Sigma_u^+)3d\sigma_g$ state lies close to numerous vibrational thresholds of the $A\,^2\Pi_u$ state. It has been pointed out[7] that its width is smaller than that of the $4d\sigma_g$ state, in disagreement with the n^{*3} scaling factor. This narrowing probably results from an interaction both with the very neighboring member $m=7$ of the series $(A\,^2\Pi_u)nd\pi_g$ converging to $v^+=3$ of the $A\,^2\Pi_u$ state and with all the members of the same series converging to the $A\,^2\Pi_u$ $v^+=2$ limit which is also close to the interloper.

V. CONCLUSION

The phenomena occurring in the vicinity of a "complex" resonance can explain in some cases the anomalies observed in the widths or in the intensities of an autoionized Rydberg series. Using our MQDT treatment, it is then possible to return to the unperturbed quantities which satisfy the usual laws (for example, the n^{*3} scale rule for the widths). This is analogous to the deperturbation performed in the case of perturbed discrete levels, but in the case of autoionized states, besides the energy shifts and the line intensities, supplementary information comes from the widths and the shapes of the resonances. Note that the occurrence of such complex resonances is independent of the nature of the open channel. In the case of a dissociative continuum, similar effects could appear near a dissociation limit. Finally, one can hope that the optical-optical double resonance (OODR) technique combined with the multiphoton ionization (MPI) spectroscopy will permit more detailed observation of numerous complex resonances in molecules. A model in which the autoionizing levels are assumed to be reached in such OODR-MPI experiment has been treated elsewhere.[25]

---

*Laboratoire associé à l'Université Paris-Sud.

[1]U. Fano, Phys. Rev. **124**, 1866 (1961).
[2]Ch. Jungen and M. Raoult, Faraday Discuss Chem. Soc. **71**, 253 (1981).
[3]P. M. Dehmer and W. A. Chupka, J. Chem. Phys. **65**, 2243 (1976).
[4]Ch. Jungen and D. Dill, J. Chem. Phys. **73**, 3338 (1980).
[5]A. Giusti-Suzor and H. Lefebvre-Brion, Chem. Phys. Lett. **76**, 132 (1980).
[6]P. M. Dehmer, P. J. Miller, and W. A. Chupka, J. Chem. Phys. **80**, 1030 (1984).
[7]M. Raoult, H. Le Rouzo, G. Raseev, and H. Lefebvre-Brion, J. Phys. B **16**, 4601 (1983).
[8]M. J. Seaton, Proc. Phys. Soc. London **88**, 801 (1966).
[9](a) A. Giusti-Suzor and U. Fano, J. Phys. B **17**, 215 (1984); (b) *ibid.* (to be published).
[10]W. E. Cooke and C. L. Cromer (private communication); C. L. Cromer, Ph.D. thesis, University of Southern California, 1983. A similar study but restricted to the case of a broad interloper has appeared when our paper was already in press [A. M. Lane, J. Phys. B **17**, 2213 (1984)].
[11]F. M. Mies, Phys. Rev. **175**, 164 (1968).
[12]F. T. Smith, Phys. Rev. **118**, 349 (1960).
[13]E. P. Wigner, Phys. Rev. **98**, 145 (1955).
[14]K. T. Lu and U. Fano, Phys. Rev. A **2**, 81 (1970).
[15]J. M. Lecomte, thèse, University of Orsay, 1983; J. M. Lecomte and E. Luc, J. Phys. B (to be published).
[16]F. Gounand, T. F. Gallagher, W. Sandner, K. A. Safinya, and R. Kachru, Phys. Rev. A **27**, 1925 (1983).
[17]U. Fano, Phys. Rev. A **2**, 353 (1970).
[18]K. A. Safinya and T. F. Gallagher, Phys. Rev. Lett. **43**, 1239 (1979).
[19]R. S. Berry, J. Chem. Phys. **45**, 1228 (1966).
[20]H. Lefebvre-Brion and A. Giusti-Suzor, in *Electron-Molecule Collisions,* edited by J. Hinze (Plenum, New York, 1983), p. 215.
[21]M. Ogawa and Y. Tanaka, Can. J. Phys. **40**, 1593 (1962).
[22]P. K. Carroll, J. Chem. Phys. **58**, 3597 (1973).
[23]E. S. Chang and K. Yoshino, J. Phys. B **16**, L581 (1983).
[24]D. Stahel, M. Leoni, and K. Dressler, J. Chem. Phys. **79**, 2541 (1983).
[25]A. Giusti-Suzor and H. Lefebvre-Brion, in Photophysics and Photochemistry Above 6 eV (Elsevier, Amsterdam, in press).